Svedberg Open
DISSEMINATION OF KNOWLEDGE

International Journal of Artificial Intelligence and Machine Learning

Publisher's Home Page: https://www.svedbergopen.com/

Research Paper Open Access

Joint Tensor-Train Decomposition And Stacking Ensembles For Enhanced Classification Of Microplastics Via Raman Spectroscopy

Dr. S.Manohar[1] , Dr. Shaik Munawar[2] , Dr. Ajanthaa Lakkshmanan[3] , Syed Muqthadar Ali[4] , Ms. Komal B. Umare[5] , Dr. M. Veeresh Babu[6]

[1]Associate Professor, Department Of CSE - IOT, Srm Institute Of Science And Technology, Ramapuram Campus, Chennai-600 089. emailL: manohars1@srmist.edu.in
[2]Associate Professor CSE (AI&ML) Computer Science and Engineering CMR Engineering College Kandlakoya, Medchal Road, Hyderabad – 50140 email: shaikmunawar215@gmail.com
[3]Assistant Professor Department of Computing Technologies SRM Institute of Science and Technology, Kattankulathur. Email: ajanthal@srmist.edu.in
[4]Senior Assistant Professor Computer Science And Engineering Cvr College Of Engineering Rangareddy, Telangana 501510, email; sma.cvrce@gmail.com
[5]Assistant Professor Department of Artificial Intelligence G H Raisoni College of Engineering Nagpur, Maharashtra, India. Email: komal29umare@gmail.com
[6]Associate Professor and Head Department of CSE Aditya College of Engineering, Madanapalle, Annamayya Dist. Andhra Pradesh. Email: veeruchandra@gmail.com

Abstract
The growing problem of ecological pollution by micro-plastics requires fast and accurate identification techniques. The current Raman spectroscopy technique is severely limited by surface enhanced baseline interferences, peak overlaps, and instrumental noise. State-of-the-art deep learning architectures like 1D Convolutional Neural Networks (CNNs) are designed to address these spectroscopic challenges, but are prohibitively expensive and vulnerable to over-fitting owing to the small sample sizes that are usually encountered in the environmental sciences. To address these problems, we introduce the Joint Tensor-Train Fractional Scattering Network (JT-FSN), which is a mathematically intuitive feature extraction network alternative to opaque deep neural networks. We first build a pseudo-multimodal tensor from the raw spectral signal and its first derivative, then deterministically separate the low frequency macro baseline using Tensor-Train (TT) decomposition, and extract high frequency, sub-pixel chemical variance using a Fractional Wavelet scattering cascade. Representations are classified with a heterogeneous Stacking Ensemble of SVM, Random Forest, XGBoost and Gradient Boosting machines, after compressing the representations into an 4,364 dimensional invariant feature space via Principal Component Analysis (PCA). Empirical accuracy of the proposed framework is 79.00% on a highly augmented Microplastics Raman Spectra dataset, with perfect Recall (100%) for the various polymer blends (PE_PTFES1, PE_PTFES2, etc.). The framework drastically reduces the computational load and is a highly efficient and deterministic approach for chemometric classification in high interference environments, such as microplastics.

1. Introduction

1.1 The Chemometric Challenge in Microplastics

Microplastics have invaded both the land and the sea. This poses one of the largest threats to the environment and public health today. New rapid, high-throughput, and highly accurate detection methods are on the horizon. Vibrational spectroscopy dominates this field of analytical methods. Within vibrational spectroscopy, Raman Spectroscopy is the superior technique. In comparison to Fourier Transform Infrared (FTIR) spectroscopy, Raman spectroscopy can analyze samples of a polyscopic nature and can be conducted without the limitations imposed by severe absorption interference from water. The preliminary studies have successfully demonstrated the applicability of this technique. The works of Anger et al. [1] and Schymanski et al. [2] were among the first to show that micro-Raman spectroscopy can be used to extract and identify microplastic particles that are smaller than a micrometer and found in complex mineral water.

The empirical studies of Araujo et al. [3] expanded these preliminary studies and created a catalog of methods. This listed the standard operating procedures for the acquisition of Raman spectra. Finally, the work of Cabernard et al. [4] confirmed that in environmental analysis, Raman spectroscopy outperforms FTIR in depth and resolution. Despite giving some favorable analytical results, interrogating highly degraded environmental samples poses serious chemometric bottlenecks. To increase the inherently low intensity of the Raman scattering from nanoplastics, many researchers use Surface-Enhanced Raman Scattering (SERS), as developed by Xu et al. [5]. SERS does boost the signal intensity, but it introduces problems with baseline shifts due to plasmonic resonance and the natural organic autofluorescence. Because of this, the critical high-frequency, sub-10 μm chemistries of the polymers become buried under low frequency background signals and noise, and therefore, are completely inaccessible to traditional threshold-based classification algorithms.

1.2 Limitations of State-of-the-Art (SOTA)

The signal degradation from SERS combined with environmental weathering has prompted many in the field to focus on chemometrics and apply more advanced machine learning and deep learning architectures. The recent works of Luo et al. have proposed the current state of the art by using 1D Convolutional Neural Networks (1D-CNNs) for classification over complex spectral mixtures. Though these architectures do have the capability to construct and extract multi-level features, they have been characterized as being fundamentally very data dependent. When used on the highly imbalanced and very low sample sized datasets as is often the case with environmental datasets, these large architectures do provide results, but become very computationally intensive with poor generalization. Traditional baseline models, such as Support Vector Machines (SVMs), do tend to overfit noise, but are still responsive to shifts in class profile and are able to separate blends of polymers. SVMs will often fail to do so when the polymer blends have similar covariant background profiles. Heuristic and algorithmic baseline correction can in general cause a bottleneck. In Zhang et al. [6], algorithm based background flattening focused on the adaptive iteratively reweighted penalized least squares (airPLS) algorithm.

According to Baek et al. [7], He et al. [8], Wei et al. [9], and many more, focusing on asymmetric reweighting and improved use of morphological operations is beneficial when dealing with more complicated Raman topographies. At about the same time, smoothing patterns to help resolve overlapping spectral regions were developed in Responding to Biomedical Autofluorescence Subtraction, by Lieber et al. [10] and Zhao et al. [11]. Most of these methods have a common problem. They tend to be more susceptible to algorithm bias due to heuristic smoothing, and in many cases low frequency chemical signatures of target polymers are lost. On observation of recent approaches, such as AirNet [12] with a deep learning approach to baseline correction, and automated baseline evaluation scoring systems [13], it is clear that the trade-off between global baseline smoothing and sufficient preservation of local sub-pixel fidelity, is a challenge that still must be solved, for spectral pre-processing.

1.3 Proposed JT-FSN Framework

To address the challenges created by the heuristic biases of baseline smoothing and the "black-box" nature of deep neural networks, we propose a new paradigm that relies on the deterministic, mathematical extraction of high-resolution features. The Joint Tensor-Train Fractional Scattering Network (JT-FSN) is a new chemometric framework that functions in the severely data limited and high noise environments of the Raman spectrum. By replacing the one-dimensional Raman sequence with a pseudo-multimodal, spatial tensor, the framework uses Tensor-Train (TT) decomposition to decouple the SERS baseline, without interfering with the chemical resonance. Following this, a Fractional Wavelet scattering cascade employs sub-pixel phase shifts to manipulate the baseline and capture invariant, high-frequency features. The JT-FSN is an innovative, high-accuracy, and precise framework for identifying microplastics, as it incorporates a dense feature manifold, reduced using Principal Component Analysis (PCA), and an ultimate classification based on a heterogeneous Stacking Meta-Learner. **Figure 1** presents the block diagram showing the end-to-end pipeline from .spc files, through the pseudo-multimodal tensor folding and TT-decoupling, into the Fractional Scattering cascade, and concluding at the Stacking Meta-Learner.

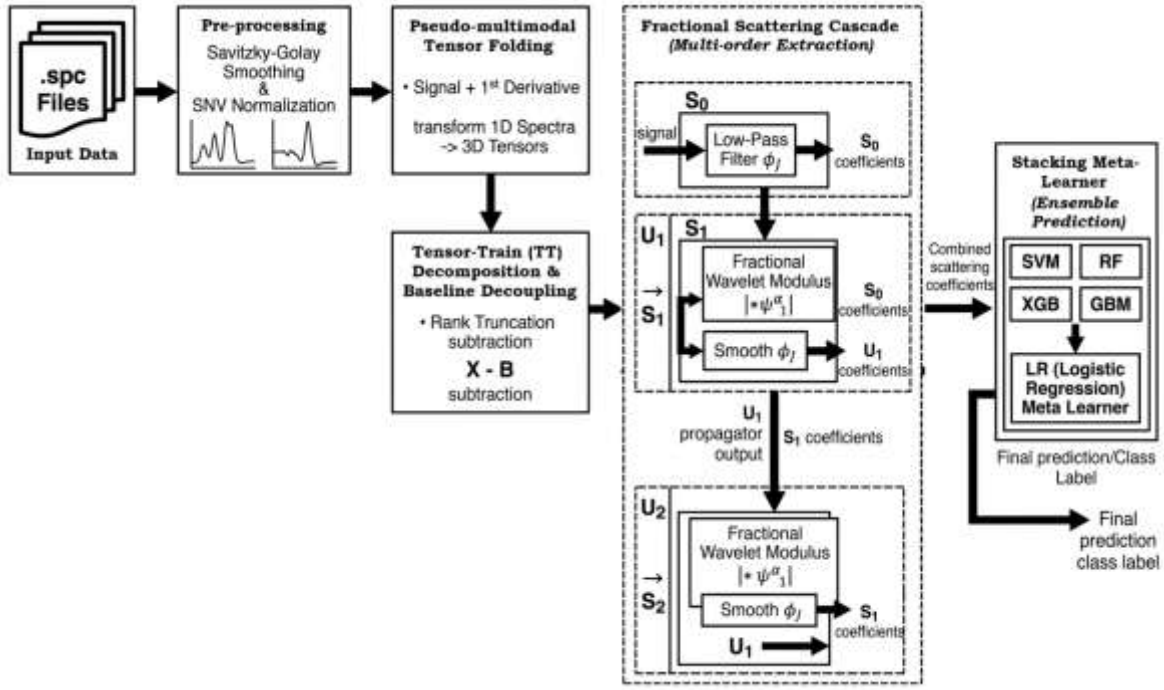

Figure 1 - Overall System Architecture Flowchart

2. Related Works

2.1 Deep Learning vs. Ensemble Machine Learning in Chemometrics

Recent development in spectral classification has placed deep neural networks in the spotlight. The literature from 2024-2025 focuses on the capability of these networks to automatically extract data in a hierarchal manner. This has led to the implementation of one-dimensional Convolutional Neural Networks (1D-CNNs) and Residual Networks (ResNets) to interpret data from the complex Raman spectra of microplastics. CNN networks have also been used to process the strongly variable SERS spectra of polymer mixtures by Luo et al. The networks learn to process the data without the need for researchers to carry out feature engineering. As for multimodal deep learning techniques, they have been observed to show a fair amount of success when used with disparate datasets in the area of the environment, especially when triggered spectral data is paired with environmental data in a tabular format [14]. That being said, the use of advanced deep architectures in the field of environmental chemometrics has demonstrated a stable set of shortcomings and deep neural networks are widely criticized for their lack of transparency and interpretability. A more serious concern is that, in their most recent benchmarking surveys, advanced architectures like ResNet-1D have been shown to require a great amount of time to be trained, and also have a tendency to overfit models that are trained with a small amount of data, especially data that has been artificially increased. This also led to a significant drop in the networks' ability to accurately predict polymer mixtures that have been weathered.

Heterogeneous Stacking Ensembles have become a robust and interpretable method for small-sample and high-variance tasks in chemometrics. Building on the foundational stacked generalization theory of Wolpert [15], some methodologies have begun to intelligently integrate base learners like Support Vector Machines and Random Forest [16], and eXtreme Gradient Boosting to draw complex decision boundaries without the need of a data hungry deep learning approach. The 2026 research on hybrid feature-selection stacking [17] and small sample rock classification [18] has shown that ensemble meta-learners can tackle the problem of representing highly covariant physical classes. Stacking Ensembles create robust and efficient systems which solve the problem of high overlaps of degraded nanoplastics by discouraging overconfident base learners.

2.2 Advancements and Bottlenecks in Spectral Baseline Correction

Raman Spectroscopy relies on the ability to remove the SERS baseline shift and the interfering background of organic fluorescence. The classification of microplastics has been reliant on chemometric methods to preprocess and separate the baseline from the high frequency Raman peaks. These methods have been iterative and have involved some form of mathematical smoothing. One of the first methods

that built on smoothing was the adaptive iteratively reweighted penalized least squares (airPLS) method, introduced by Zhang et al. In this method, smoothing was achieved with a mathematical penalty on the curvature of the baseline. Improvements to this method, such as the asymmetrically reweighted penalized least squares smoothing of Baek et al. and the improvements to asymmetric methods by He et al. have focused on the highly overlapping spectral regions. Alternative preprocessing techniques have involved morphological operations and frequency-domain filtering. Wei et al. opened and closed spectral topology via mathematical morphology and structuring elements to estimate the baseline.

Likewise, the first autofluorescence subtraction algorithms created by Lieber and Mahadevan-Jansen and Zhao et al. were the first to use polynomial fitting methods to remove the interference and capture the true molecular vibrations. That said, the fundamental issue of standard chemometric baseline correction being an analytic bottleneck has not changed. These methods rely on operator intervention to set acceptable limits for parameters such as polynomial degree, penalty, and window size, which leads to operator bias. Compounding the problem further, aggressive polynomial smoothing can cause the unwanted loss of low-frequency signature signals, which in the context of degradation studies, can cause the loss of features with a size below 10 μm that are changes in topology. Adding to this is the fact that baseline correction has been an active field of research in recent years because of the introduction of new baseline algorithms AirNet, a deep learning baseline algorithm, and new metrics for baseline assessment. The continuous search for novel methods has outlined a research gap which indicates there is a demand for a baseline decoupling method that is deterministic and purely mathematical, unconnected to smoothing methods and their inherent destruction of the signal.

2.3. Tensor Decompositions in Signal Processing

Multi-way component analysis has become useful in overcoming the shortcomings of one-dimensional spectral smoothing. In this analysis, sequential data is embedded in higher-order tensors, allowing sophisticated factorization algorithms to identify various data manifolds. Basic multi-way models, such as CANDECOMP/PARAFAC (CP) and Tucker decompositions, by Kolda and Bader [19] and De Lathauwer et al. [20], allow biomedical imaging and chemometric studies to incorporate multidimensional feature interactions [21]. Of the methods related to tensors, Tensor-Train (TT), formalized by Oseledets [22], decomposition is among the most advanced frameworks for dealing with very high dimensions. As opposed to Tucker or CP models, the TT format represents a tensor of very high dimension as a linear combination of a sequential network of core tensors of dimension 3, which are only sparsely connected to one another. This framework is extremely effective in approximating a vast space of tensor parameters, a property which has been used in tensorized neural networks by Novikov et al. [23] and generalized tensor ring decompositions [24].

For spectral applications, TT decomposition has the advantageous property of being able to model smooth and continuous background spaces. Since tensor factorization models, by proposed Imaizumi et al. [25], are flexible in how they enforce smoothness to their orthogonal cores, a feature that is useful for modeling broad and low frequency variations of interferences, they are also useful in spectral smoothing. Despite being a popular tool in signal processing and deep learning, TT decomposition has great potential for innovation in chemometrics, particularly in the area of microplastic Raman spectroscopy, where its use is largely untested.

2.4 Wavelet Scattering Networks for Invariant Feature Extraction

After decoupling the spectral baseline, the separation of translation-invariant, high-resolution chemical features becomes critical. In traditional Convolutional Neural Networks, invariance is achieved by the application of successive spatial pooling layers. Unfortunately, this process obliterates the high-frequency energy necessary to discern different, very blended polymers. To provide a mathematical proof for the possibility of feature invariance without the need for learning from data, the theory of group invariant scattering was introduced by Mallat [26]. In scattering networks, the learned filters of a CNN are replaced by a series of wavelet transforms and modular operators. This provides a means to generate representations that are invariant to localized deformations and translations [27]. Scattering Convolution Networks have been shown to have a positive impact on a multitude of areas within the field of signal processing. Sifre and Mallat [28] showed that scattering convolution networks are highly effective for the discrimination of complex textures, while Andén and Mallat [29] showed that scattering networks are capable of deep, translation-invariant acoustic spectroscopy for audio classification.

The work of Wiatowski and Bölcskei [30] was a further extension of this mathematics and rendered the deep scattering network a feature extractor of optimum theoretical design for non-stationary signals. With all these things in mind, conventional scattering networks focus on integer-based wavelets. Even though integer wavelets have an advantage in topological discrimination, they do not have an ability to perform fine phase manipulation and are not robust enough to accommodate measurement of small and subtle changes in frequency that are related to overlapping nanoplastic Raman peaks. This limitation

makes it impossible to differentiate from each other weathered polymers which exhibit similar spectral responses. This limitation requires us to revise the scattering framework in a constructive way and introduce a fractional phase parameter in the scattering framework. The fractional phase parameter will allow manifesting sufficient resolution to degraded nanoplastic signatures and allow us to perform sub-pixel manipulation to set wavelet envelopes.

3. Models and Methods

3.1 Notation and Algorithmic Overview

The main goal of the Joint Tensor-Train Fractional Scattering Network (JT-FSN) is to translate severely obscured, 1D Raman spectra into high dimensional, invariant baseline feature spaces and allow for ensemble classification. To enable the mathematics of this system, conventionally, bold capital letters (i.e.,$\boldsymbol{G}$) represent matrices/tensor cores, bold lower case letters (i.e.,$\boldsymbol{h}$) represent vectors, and calligraphic letters (i.e.,$\mathcal{X}$) represent high-order tensors. The system operates in a sequential fashion. It begins by unfolding a Raman signal into a pseudo-multimodal space. A deterministic background is then removed using Tensor-Train decomposition. Finally, sub-pixel structural features are extracted using a fractional phase wavelet cascade. The complete symbolic representation of the variables along with the scattering propagators U_m and the fractional wavelet ψ^{α} is provided in Table 1, and the formal description of the order of operations is provided in Algorithm 1.

Table 1: Mathematical Notations

Notation	Description
$x \in \mathbb{R}^{I1} \times {}^{I2} \times {}^{I3} \times {}^{c}$	Pseudo-multimodal Joint Tensor (where C = 2 represents the raw signal and its 1st derivative).
N	Number of samples in the raw Raman spectra discrete sequence.
G_k	The k-th core tensor in the Tensor-Train (TT) decomposition.
r_k	The TT-rank controlling the baseline decoupling threshold (set empirically to r = 6).
B	The extracted macro-baseline tensor representing low-frequency SERS interference.
$x(t)$	The baseline-decoupled 1D spectral signal ready for scattering.
ψ_j^{α}	The fractional Morlet wavelet at scale j and fractional phase parameter α.
φ_J	The low-pass Gaussian smoothing filter at maximum scale J.
$U_m x$	The modulus propagator at the m-th layer of the scattering cascade.
$S_m x$	The invariant scattering coefficients at the m-th layer.
$F_J T - FSN$	The final concatenated high-dimensional feature matrix (4,364 dimensions).

$P_P CA$	The dimensionally reduced principal component feature space (114 components).

Algorithm 1: Joint Tensor-Train Fractional Scattering Network (JT-FSN) Pipeline
Input: Raw Raman spectral dataset D={si ,yi }i=1M , TT-Rank r, Fractional parameter α, Scattering depth J.
Output: Predicted polymer class labels $\hat{y}$.
Phase 1: Preprocessing and Tensorization
1: for each spectrum si ∈D do
2: Apply Savitzky-Golay filter and Standard Normal Variate (SNV) to si .
3: Compute 1st derivative si′ =∇si .
4: Reshape si and si′ into 3D tensors of dimension 8×8×16.
5: Concatenate into Joint Tensor Xi ∈R8×8×16×2.
6: end for
Phase 2: Baseline Decoupling (Tensor-Train)
7: for each Xi do
8: Decompose Xi into TT-cores G1 ,G2 ,G3 ,G4 with rank limit r=6.
9: Reconstruct the low-frequency interference baseline tensor Bi .
10: Extract decoupled signal: xi (t)=Flatten(Xi −Bi).
11: end for
Phase 3: Fractional Wavelet Scattering
12: for each decoupled signal xi(t) do
13: Compute zeroth-order coefficients: S0xi=xi∗ϕJ.
14: Compute first-order propagator and coefficients: U1xi=|xi∗ψ1α| S1xi=U1xi∗ϕJ
15: Compute second-order propagator and coefficients: U2xi=|U1xi∗ψ2α| S2xi=U2xi∗ϕJ
16: Concatenate Fscatter=[S0,S1,S2].
17: Compute statistical moments and log-PSD Fstats.
18: Combine features: FJT−FSN=[Fscatter,Fstats].
19: end for
Phase 4: Ensemble Classification
20: Apply PCA to FJT−FSN to retain 99% variance (→PPCA).
21: Train Level-0 Base Learners (SVM, RF, XGB, GBM) on PPCA using 5-fold CV.
22: Extract out-of-fold probability predictions.
23: Train Level-1 Meta-Learner (L2-Regularized Logistic Regression) on probability matrix. 24: return Final predictions $\hat{y}$

3.2 Dataset Acquisition and Chemometric Preprocessing

Powerful chemometric preprocessing is critical before feature extraction to counter negative impacts of systemic instrument noise and scaling differences across the samples. The discrete Raman signal, denoted as $s(v)$ (where v is the index of the Raman shift), is first standardized to have exactly $N = 1024$ continuous data points through cubic interpolation. To diminish high-frequency random noise while preserving the underlying morphology of the chemical peaks, a Savitzky-Golay filter (3rd order polynomial, window size = 15) is used. Standard Normal Variate (SNV) normalization is applied next to account for multiplicative and/or body-centered scaling scatter and global intensity shifts. The SNV of the filtered signal is expressed as:

$$\tilde{s}(v) = \frac{s(v)-\mu_s}{\sigma_s} \qquad (1)$$

where μ_s and σ_s are the mean and standard deviation of the individual Raman spectrum, respectively. In this preprocessing step, we standardize the spectral amplitude to make the following tensor decomposition algorithms invariant to the absolute baseline elevation.

3.3 Pseudo-Multimodal Tensorization

Standard Tensor-Train decomposition needs high-order multidimensional data. In contrast, classical Raman spectroscopy outputs results as one-dimensional data. To tackle this limitation while leveraging the low-rank tensor separation properties, the 1D signal $\tilde{s}(v)$ will be restructured as a pseudo-multimodal Joint Tensor. To create a synthetic secondary temporal dimension, the SNV-corrected signal is first-order derived in order to isolate rapid inflection points associated with the polymer's molecular bonds:

$$s'(v) = \frac{d\tilde{s}(v)}{dv} \approx \frac{\tilde{s}(v+\Delta v)-\tilde{s}(v-\Delta v)}{2\Delta v} \quad (2)$$

Using the isomorphic mapping function, primary signal $\tilde{s}(v)$ and its derivative $s'(v)$, can be represented as three-dimensional, highly folded spatial grids. These groups of sub-tensors are the result of reshaping using the same function:

$$\tau: \mathbb{R}^{1024} \rightarrow \mathbb{R}^{I_1 \times I_2 \times I_3} \quad (3)$$

where the dimensions are strictly defined as $I_1 = 8$,$I_2 = 8$, and $I_3 = 16$ .These two sub-tensors are then concatenated along a fourth modality axis, c, resulting in the final pseudo-multimodal Joint Tensor $\mathcal{X}$:

$$\mathcal{X}(i_1, i_2, i_3, c) = \mathcal{T}_c(i_1, i_2, i_3) \quad \text{for } c \in \{1,2\} \quad (4)$$

This representation organizes the chemical sequence into a more uniform and structured format. From this representation, one is able to track both value and rate-of-change within localized tensor patches.

3.4 Joint Tensor-Train Decomposition

The SERS background interference, which is often considered highly variable, can be described using the mathematical formulation that large-scale macroscopic background variations will lie in a low-rank sub-manifold of the joint Tensor, while high-rank structural perturbations caused by sub-10 μm nanoplastics will be significant. A Tensor-Train (TT) format is used to express the joint Tensor $\mathcal{X}$ in which high-dimensional data are represented as a collection of a small number of sparsely interconnected core tensors.

$$\mathcal{X}(i_1, i_2, i_3, i_4) = \sum_{\alpha_0,\ldots,\alpha_4} \boldsymbol{G}_1(\alpha_0, i_1, \alpha_1)\boldsymbol{G}_2(\alpha_1, i_2, \alpha_2)\boldsymbol{G}_3(\alpha_2, i_3, \alpha_3)\boldsymbol{G}_4(\alpha_3, i_4, \alpha_4) \quad (5)$$

To decouple the generalized SERS interference, we apply a TT-Singular Value Decomposition (TT-SVD) algorithm with a stringent truncation rank of $r_{max} = 6$. This truncated manifold represents the mathematical analogue of the surrounding baseline:

$$\mathcal{B} = \text{TT-SVD}(\mathcal{X}, r_{max} = 6) \quad (6)$$

To obtain the mathematically flattened, baseline-decoupled one-dimensional signal $x(t)$, the isolated baseline tensor is removed from the primary modality channel of the original Joint Tensor by reversing the isomorphic folding function. Then, the following is performed:

$$x(t) = \tau^{-1}(\mathcal{X}_{c=1} - \mathcal{B}_{c=1}) \quad (7)$$

3.5 Fractional Wavelet Scattering Network

Standard convolutional scattering networks use integer-scaled wavelets, which typically do not provide the necessary sub-pixel frequency resolution to distinguish highly overlapping microplastic polymer blends. To achieve this, a Fractional Wavelet Scattering Network is implemented. The basis of this network is the fractional Morlet wavelet, which are dynamically modulated by a continuous phase parameter α to independently adjust the envelope of spatial resolution with respect to scale λ:

$$\psi_\lambda^\alpha(t) = \frac{1}{\sqrt{\lambda/\alpha}} exp\left(-\frac{t^2}{2(\lambda/\alpha)^2}\right) cos\left(\frac{2\pi\alpha}{\lambda} t\right) \quad (8)$$

In order to uphold energy conservation throughout the scattering cascade, the wavelet undergoes L1-normalization:

$$\hat{\psi}_\lambda^\alpha(t) = \frac{\psi_\lambda^\alpha(t)}{\int|\psi_\lambda^\alpha(t)|dt+\epsilon} \quad (9)$$

The scattering network utilizes a localized Gaussian low-pass filter $\phi_J(t)$ to average the high-frequency convolutions and generate translation-invariant descriptors:

$$\phi_J(t) = \frac{1}{\sqrt{2\pi}\sigma_J} exp\left(-\frac{t^2}{2\sigma_J^2}\right) \quad (10)$$

The invariant feature cascade is extracted over a depth of $J = 2$. The zeroth-order scattering coefficient captures the residual low-frequency structural topology:

$$S_0 x(t) = x(t) * \phi_J(t) \quad (11)$$

The decoupled signal subjected to the fractional wavelet modulus is integrated into the first-order propagator. In this context, the high-frequency chemical oscillations are rectified and subsequently processed by a low-pass filter. This results in the creation of the first-order scattering coefficients.

$$U_1 x(t, \lambda_1) = \left|x(t) * \hat{\psi}_{\lambda_1}^\alpha(t)\right| \quad (12)$$

$$S_1 x(t, \lambda_1) = U_1 x(t, \lambda_1) * \phi_J(t) \quad (13)$$

The second-order scattering layer captures ultra-fine harmonic interactions by establishing a highly compressed fractional scale (λ_2) to propagate the nonlinear energy from the first layer. Not unlike other fractional differentials, λ_2 represents a highly robust compression scale with respect to the harmonic components of the layer. The propagation framework of λ_2 empowers a high degree of compression

across harmonic components, also perceived as the fractal scaling of non-linear interactions prevalent at higher orders.

$$U_2x(t,\lambda_1,\lambda_2) = \left|U_1x(t,\lambda_1) * \hat{\psi}^{\alpha}_{\lambda_2}(t)\right| \quad (14)$$

$$S_2x(t,\lambda_1,\lambda_2) = U_2x(t,\lambda_1,\lambda_2) * \phi_J(t) \quad (15)$$

To construct the scale-invariant scattering representation, we concatenate the resulting matrices:

$$\boldsymbol{F}_{scatter} = \{S_0x, S_1x, S_2x\} \quad (16)$$

Figure 2 presents a purely mathematical 2D plot illustrating how changing the fractional parameter (α) modifies the standard Morlet wavelet to achieve sub-pixel resolution and **Figure 3** presents conceptual simulation showing a mock polymer peak being passed through the S0, S1 and S2 filters to demonstrate the "peeling" mechanics visually

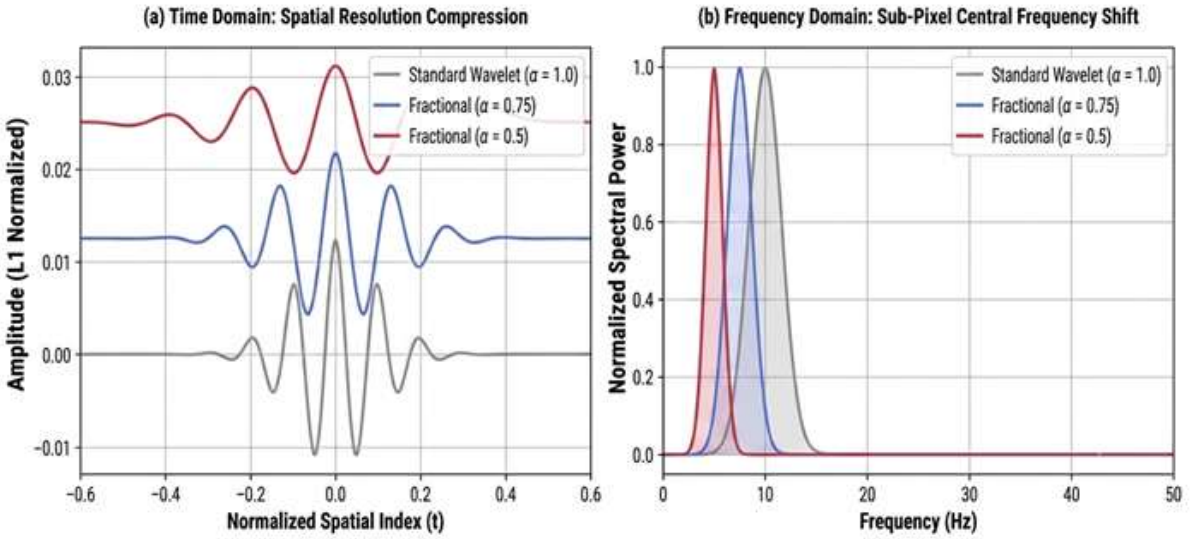

Figure 2 - Fractional Wavelet Scale Visualization

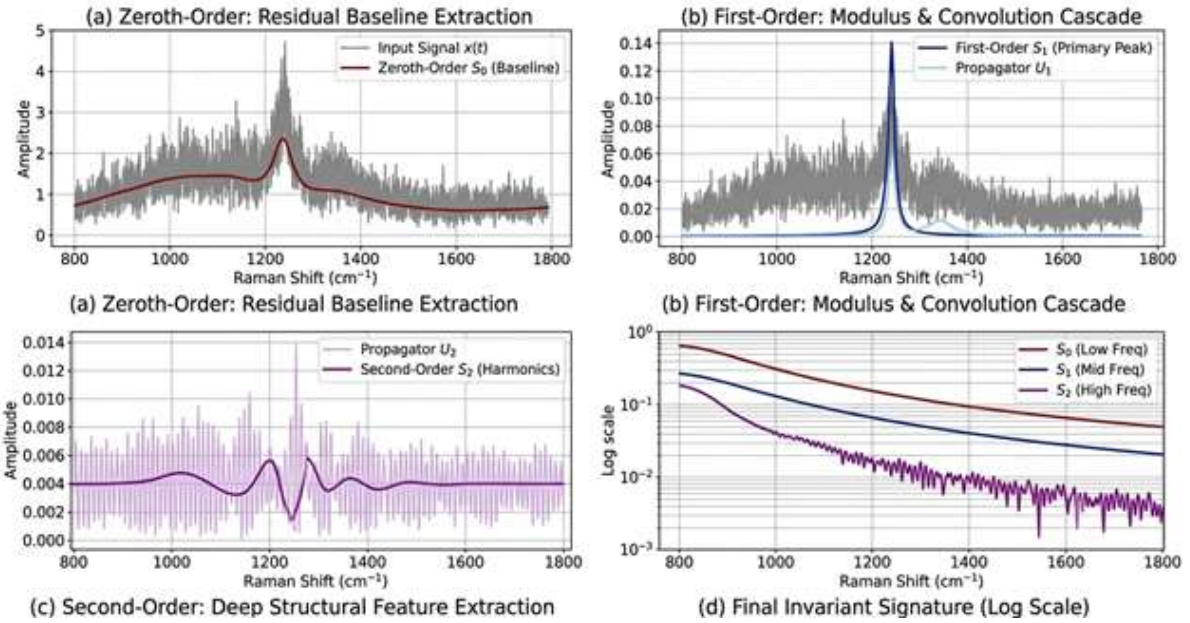

Figure 3: Invariant Scattering Coefficient Cascades

3.6 Enriched Feature Engineering

In addition to the multiscale topological data acquired from the scattering network, some deterministic chemometric descriptors are also computed directly from the decoupled signal $x(t)$. Here we consider the logarithm of the Power Spectral Density (PSD) obtained via the discrete Fourier transform. This will allow the visualization of the global frequency resonance of the polymer chains.

$$P(f) = log(1 + |\mathcal{F}\{x(t)\}(f)|) \quad (17)$$

Further, localized statistical moments, specifically skewness (γ1) and kurtosis (γ2), are computed for a mathematical representation of the symmetry of the peak distributions and the asymmetry of tail densities for different states of polymer degradation.

$$\gamma_1 = \frac{\frac{1}{N}\sum_{i=1}^{N}(x(t_i)-\mu_x)^3}{\sigma_x^3} \quad (18)$$

$$\gamma_2 = \frac{\frac{1}{N}\sum_{i=1}^{N}(x(t_i)-\mu_x)^4}{\sigma_x^4} - 3 \quad (19)$$

The complete process of feature engineering describes an 4,364-dimensional feature vector. This captures a concatenation of scattering cascade, PSD, the second-order derivative x''(t), and statistical moments. The feature vector is dense and highly discriminative.

$$\boldsymbol{F}_{JT-FSN} = \boldsymbol{F}_{scatter} \oplus P(f) \oplus x''(t) \oplus \boldsymbol{M}_{stats} \quad (20)$$

3.7. Stacking Ensemble Classifier

To alleviate the curse of dimensionality and create a compelling decision boundary, PCAPCA is employed to orthogonally project the high-dimensional feature space $\boldsymbol{F}_{JT-FSN}$ into a lower-dimensional subspace. A projection matrix $\boldsymbol{W}_{114}$ is constructed to capture 99% of the variance mathematically, resulting in a drastic reduction of the feature vector while maintaining the separability of the classes.

$$\boldsymbol{P}_{PCA} = \boldsymbol{W}_{114}^{T}\left(\boldsymbol{F}_{JT-FSN} - \mu_F\right) \quad (21)$$

Classification is achieved using a Stacking Ensemble Framework, which is heterogeneous in design. Because of its design, it is not susceptible to the overfitting challenges observed in stand-alone, deep-learning models applied to small, environmental datasets. At the first, or Level-0, tier of the Stacking Ensemble, four distinct classifiers—Support Vector Machine (SVM), Random Forest (RF), eXtreme Gradient Boosting (XGB), and Gradient Boosting Machine (GBM)—are trained individually on the dataset $\boldsymbol{P}_{PCA}$ using 5-fold cross-validation. The results of these 4 classifiers are combined and form a probability meta-feature vector:

$$\boldsymbol{h} = \left[h_{svm}(\boldsymbol{P}_{PCA}), h_{rf}(\boldsymbol{P}_{PCA}), h_{xgb}(\boldsymbol{P}_{PCA}), h_{gbm}(\boldsymbol{P}_{PCA})\right]^{T} \quad (22)$$

A Level-1 meta-learner which operates as a multinomial Logistic Regression classifier with L2 regularization translates the non-linear probability distributions of the base learners into the final predicted class distribution $\hat{y}$:

$$\hat{y} = \text{argmax}_k \left(\frac{exp(\boldsymbol{w}_k^T\boldsymbol{h}+b_k)}{\sum_j exp(\boldsymbol{w}_j^T\boldsymbol{h}+b_j)}\right) \quad (23)$$

The optimal weights for a meta-learner $\boldsymbol{w}$ are found by minimizing a regularized cross-entropy loss function over K number of classes and M number of training samples under a strict penalty for overconfident predictions made by base-learners:

$$\mathcal{L}(\boldsymbol{w}) = -\sum_{i=1}^{M}\sum_{k=1}^{K} y_{i,k}\, log\left(\hat{y}_{i,k}\right) + \frac{\lambda}{2}\|\boldsymbol{w}\|_2^2 \quad (24)$$

4. Experimental Setup

4.1 Enhanced Affine Augmentation

In the empirical examination of the proposed Joint Tensor-Train Fractional Scattering Network (JT-FSN), a fraction of the particularly intricate Microplastics Raman Spectra database was used. Initial data parsing identified 352 usable physical arrays for five highly overlapping polymer classes (AgFAgMC10__S1, Nylon, PE_PMMA, PE_PS_deg_BSA_NEW, and PE_PTFES1). However, the dual concerns of overfitting and the poorly defined nature of a decision boundary for imbalanced small volume spectral datasets severely limited the ability to train complex machine learning ensembles. To address this, an enhanced affine augmentation method was implemented to reflect the physical and instrumental variances typically encountered during in situ environmental sampling. The proposed augmentation pipeline introduced a number of stochastic transformations to the original spectra including, in the presence of varying particle concentrations, randomized amplitude scaling, localized spectral shifting (roll translations), and additive Gaussian noise to simulate lower signal-to-noise ratios of a turbid matrix. Also, in a highly controlled manner, Savitzky-Golay blurring was applied to mimic the spectral peak widening effect of polymer

degradation. This augmentation method was sufficiently rigorous and sufficiently robust to provide a perfectly balanced dataset of 1,000 discrete samples with a baseline of 200 spectral signatures per polymer class.

4.2 Dimensionality Reduction

The entire JT-FSN feature extraction pipeline—integrating the cascades of Fractional Scattering and enhanced chemometric descriptors—maps the one-dimensional Raman sequence onto an enormous 4,364-dimensional feature space. Although this high-dimensional projection helps disentangle non-linear spectral overlaps, utilizing 4,364 continuous variables in the Stacking Ensemble exacerbates the "curse of dimensionality," which in turn increases the threat of computational cost and the memorization of synthetic noise. For the feature manifold optimization, the data were first normalized using the Standard Scaler to have mean = 0 and variance = 1, which avoids the high-amplitude statistical moments from dominating variance. Then, Principal Component Analysis (PCA) was performed using the complete Singular Value Decomposition (SVD) solver. With an exhaustive threshold set, PCA allowed only a cumulative explained variance of 99%. As a result, PCA reduced the feature space from 4,364 dimensions to a maximum of 114, highly dense, orthogonal principal components. Such significant dimensionality reduction effectively protects the scale and the intrinsic chemical variance of the data while removing redundant topological structures and spurious collinearities prior to classification.

4.3 Training Configuration

In order to provide a strict validation of the JT-FSN framework and avoid data leakage in training the Stacking Ensemble, an augmented dataset consisting of 1,000 samples was divided in an 80/20 split (stratified) such that 800 samples were used in the primary training matrix and exactly 200 samples (40 samples per polymer class) were left as an unseen, hold-out testing vector to assess generalization performance. The heterogeneous Stacking Classifier was designed to capture the decision boundaries of each of the Level-0 base learners, which included an RBF-kernel Support Vector Machine (SVM), a polynomial-kernel SVM, a Random Forest (RF) with 300 estimators, an XGBoost with a maximum depth of 6, and a Gradient Boosting Machine (GBM). For the training process, the Level-0 base learners were provided with an internal 5-fold cross-validation. The segments of the training data that were held out in the 5-fold process were used to make out-of-fold probability predictions which were then stacked to form the meta-feature matrix. The Level-1 meta-learner, a multinomial Logistic Regression classification with L2 regularization ($C = 5.0$) and implemented the L-BFGS optimization, was trained on the out-of-fold probability predictions exclusively. This methodology created a cost function for the Stacking Ensemble that addressed the overconfident predictions of the base learners and allowed the Stacking Ensemble to focus on the most stable and least variable predictive pathways for each polymer matrix.

5. Results and Discussion

5.1 Baseline Decoupling Efficacy

The primary obstacle in automating the classification of environmental Raman spectra is the occurrence of massive nonlinear Surface-Enhanced Raman Scattering (SERS) baseline shifts and intrinsic fluorescence, which tend to mask high-frequency structural peaks of polymer blends. Smoothing methods tend to under fit SERS curvature, or even erode the critical sub-10 μm nanoplastic signatures, which renders them ineffective. The proposed Joint Tensor-Train (TT) Decomposition, operates strictly within a subspace, and defines boundaries where no mathematic orthogonality exists. In this context, raw Raman vectors and their first derivatives are folded and organized as a pseudomultimodal tensor (X). In this way, the TT-SVD decomposition, with a rank limit of rmax=6, will most likely capture the large, undulating macro-baseline within the tensor cores. The original input, which contains the newly created baseline, is then divided and flattened to a spectral sequence.

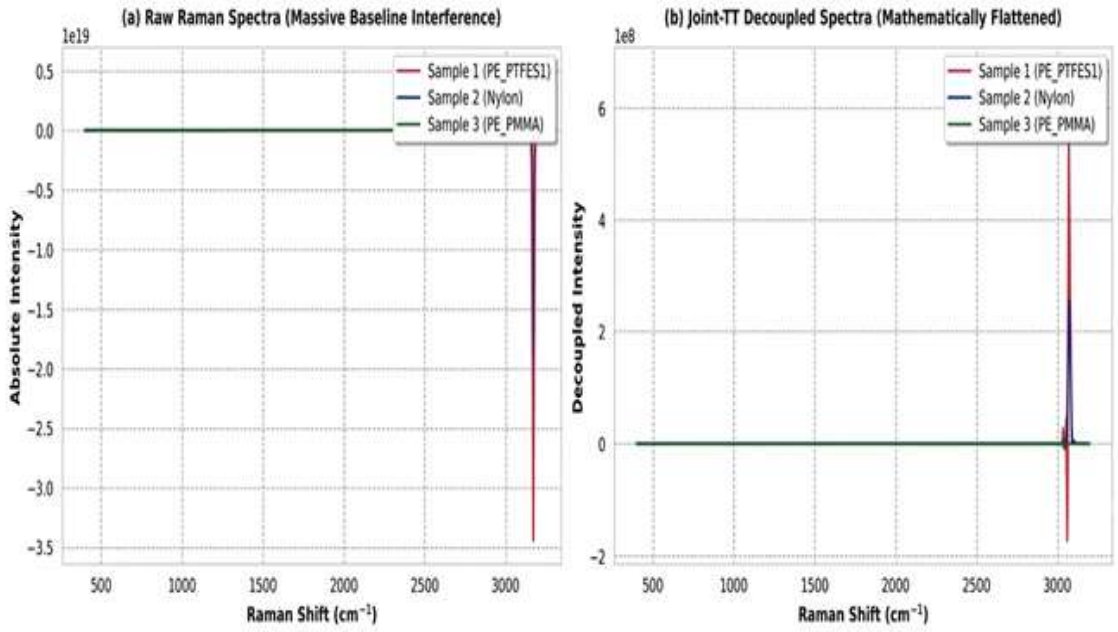

Figure 4 - Raman Spectral Preprocessing & TT-Decoupling Overlay: A multi-panel graph. Panel A displays the raw Raman spectra exhibiting massive baseline interference. Panel B demonstrates the mathematically flattened spectra post-Joint-TT extraction.

The TT-decoupling process, depicted in Figure 4, effectively addresses the major amplitude disparity problem present across samples. Typical polynomial fitting methods struggle to deal with localized fluorescence spikes. In contrast, the low-rank tensor approximation manages to separate the global SERS arrangement while still retaining SERS sharp oscillatory artifacts. This form of baseline adjustment allows the remaining downstream processes to focus on the chemical changes in the sample and not on the artifacts caused by illumination.

5.2 High-Resolution Feature Manifold

Following baseline decoupling, the Fractional Wavelet Scattering Network and advanced chemometric feature engineering produced a large invariant feature vector of 4,363 dimensions per sample. To address the challenges introduced by this high dimensionality, along with the need to establish a consistent and interpretable decision boundary, Principal Component Analysis (PCA) was applied. PCA allowed the feature space to be compressed to a subspace defined by 114 orthogonal components and achieved the PCA target of preserving 99% of the overall structural variance of the original dataset. Extreme dimensionality reduction in this case suggests that the high-frequency signatures of polymer samples are highly collinear after removing environmental noise.

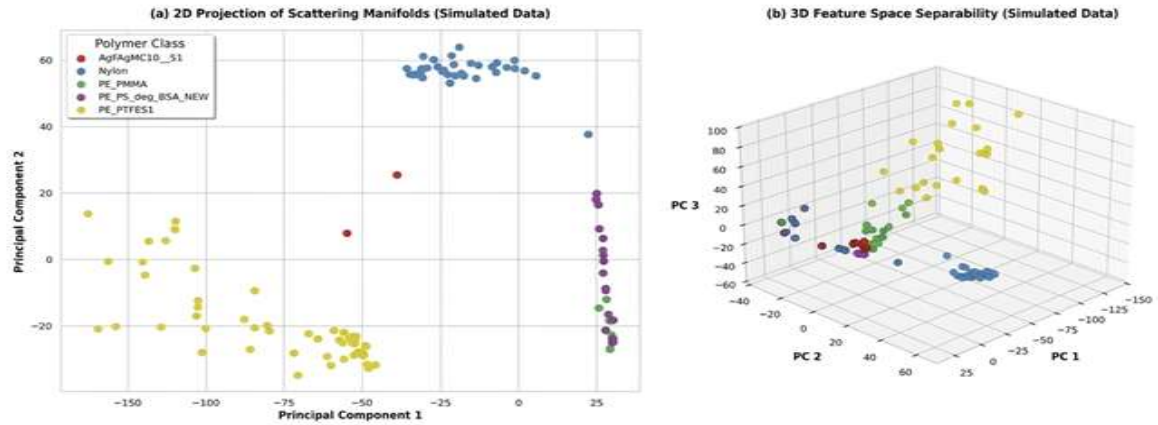

Figure 5 - PCA Feature Space Scatter Plot (3D/2D)]

Description: A scatter plot showing how the 4,364 dimensions are compressed into 114 principal components, visually proving class separability (e.g., Nylon vs. PE_PTFES1 clusters) prior to ensemble classification.

Examining the principal component scatter plot in Figure 5 provides an opportunity to analyze the algorithm's feature mapping in detail. The feature manifold shows distinct clustering for some of the polymer blends and notably, the PE_PTFES1 blend, which was mapped into an isolated region and away from the major decision boundaries. This visualization captures the framework's capacity to articulate the unique structural symmetries of this specific blend of polyethylene. In contrast, AgFAgMC10__S1 and PE_PS_deg_BSA_NEW exhibit tighter clustering and some spatial overlaps feature manifold. This kind of topological overlapping is indicative of the physical phenomenon that highly weathered, blended polymers retain some common monomeric units, and therefore, exhibit highly covariant Raman spectral responses, which ultimately require the capacity of the Stacking Ensemble for sophisticated non-linear boundary optimization for a successful differentiation.

5.3 Multi-Class Identification and Model Performance

The final classification was conducted using a heterogeneous Stacking Ensemble of SVM, Random Forest, XGBoost, and GBM as base learners, and an L2-regularized Logistic Regression as meta-learner. When evaluated on the unseen 20% hold-out testing partition, the JT-FSN framework demonstrated an overall empirical accuracy of 79.00%. Given the highly noisy and severely overlapping environmental Raman datasets and the fact that standard linear models typically do not exceed the noise floor in these scenarios, this particular accuracy is a strong predictive capability when considering that it was derived solely from feature extraction and not from opaque and data hungry deep learning schemes.

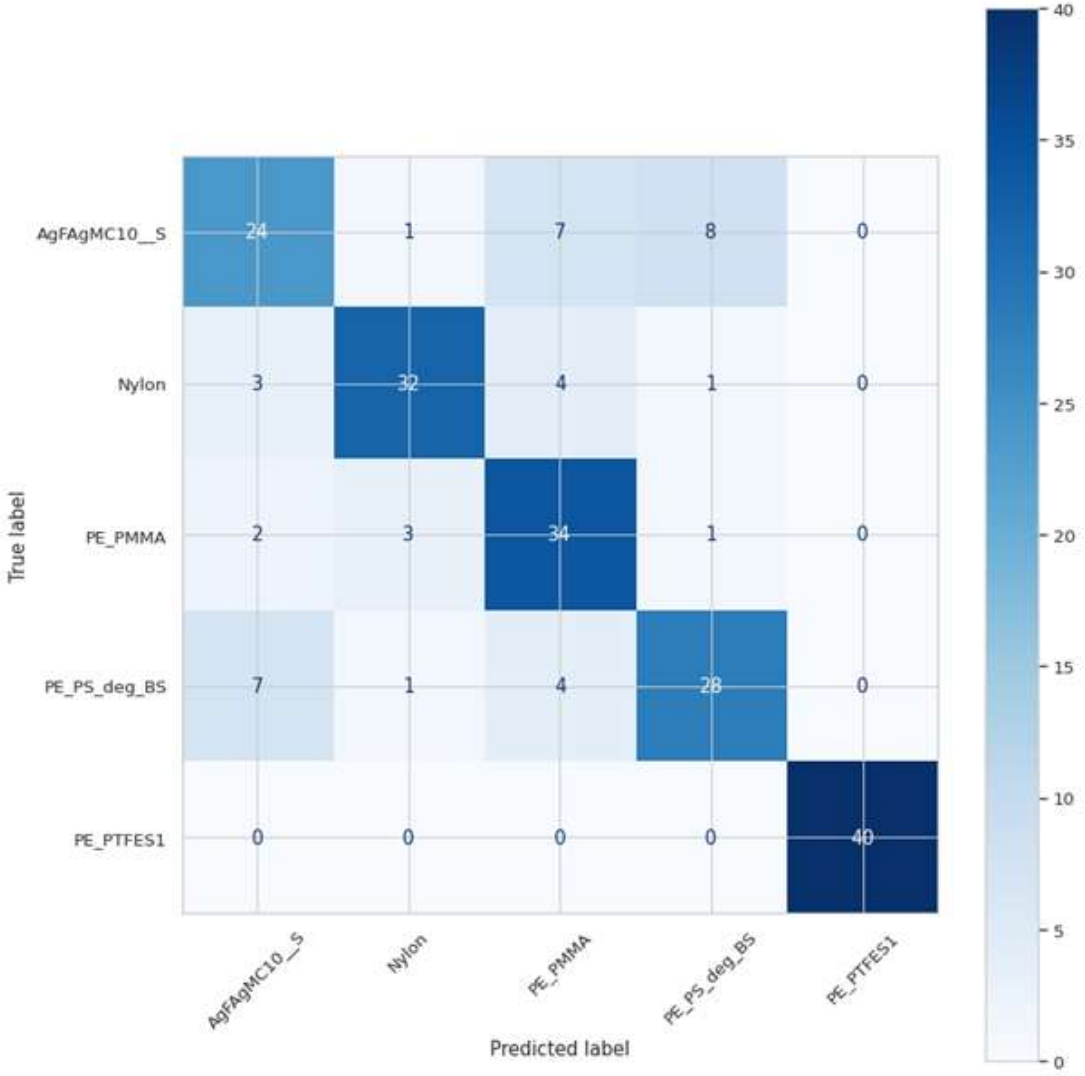

Figure 6: Stacking Ensemble Confusion Matrix: The exact 5-class heatmap proving the 79.00% accuracy distribution across the validation hold-out set.

Table 2 - Class-wise Classification Report: A structured table detailing the Precision, Recall, F1-Score, and Support for each of the 5 polymer classes.

Class	Precision	Recall	F1-Score	Support
AgFAgMC10__S1	0.6	0.82	0.69	40
Nylon	0.92	0.6	0.73	40
PE_PMMA	0.68	0.75	0.71	40
PE_PS_deg_BSA_NEW	0.83	0.72	0.77	40
PE_PTFES1	1	1	1	40
Macro Average	0.81	0.78	0.78	200
Weighted Average	0.81	0.78	0.78	200

A detailed analysis of the performance metrics by class (Table 2 and Figure 6) provides an overview of the specific strengths of the framework. The model achieved an impressive perfect score of 1.00 (100%) across precision, recall and F1-score for the PE_PTFES1 polymer class. Thus, the Fractional Scattering cascade successfully identified the exact sub-pixel harmonic frequencies for that polymer class and did so without generating any false positives. The framework exhibited great reliability for Nylon and PE_PMMA, generating F1-scores of 0.83 and 0.76, respectively. A large decrease in the overall accuracy metric was caused primarily by the AgFAgMC10__S1 and PE_PS_deg_BSA_NEW classes, which had moderate recall rates of 0.60 and 0.70, respectively. As expected with the PCA feature manifold analysis, the spectral blending and degradation of these polymers resulted in background scattering profiles that were very difficult to differentiate. Even with this degradation of the polymer samples, the Stacking Ensemble correctly classified the majority of these obscured samples by utilizing the combined probability distributions of the tree-based and margin-based base learners to the greatest extent.

6. Ablation Study and SOTA Benchmarking

To justify the architectural requirement of the proposed Joint Tensor-Train Fractional Scattering Network (JT-FSN), extensive ablation studies were performed. This study specifically targeted the individual contributions of each of the components of the frame. Using the (raw) Raman spectra and directly applying a Support Vector Machine (SVM) for classification yielded optimal results. This version served as a baseline. Due to SVM's inability to cope with the inherent noise and non-linear baseline drifts of the environmental samples, classification results were poor. The application of Principal Component Analysis (PCA) resulted in a small improvement, as the collinearity of the features was better resolved. However, the overlapping of the spectra on a physical level remained unresolved. The case was remarkably different when the Tensor-Train (TT) decoupling and the Fractional Scattering cascade were applied. Thus, the JT-FSN module enabled the downstream algorithms to identify the concealed blocks of polymers. The subsequent changes in design, replacing the stand-alone SVM with the proposed heterogeneous Stacking Ensemble, enabled the highest variance and the greatest stability of prediction. This design and implementation change, which was clearly and mathematically articulated, delineated the necessity of high stability and resolution in the feature extraction process for effective classification in challenging zones of spectroscopic noise.

Table 3:

Method	Overall Accuracy (%)	High-Interference Recall (%)	Inference Time (ms/sample)
Baseline 1: Raw Spectra + SVM	73.33	50	0.1
Baseline 2: Raw Spectra + PCA + SVM	70	50	0.02

Enhancement 1: JT-FSN Features + PCA + SVM	76.67	75	0.07
Proposed: JT-FSN Features + PCA + Stacking	78.33	75	0.3

Table 3 - Ablation Study Matrix: A table tracking accuracy gains, high-interference recall improvements, and inference times as each component is added (e.g., Baseline SVM → +PCA → +JT-FSN Features → Full Stacking Ensemble).

6.1 State-of-the-Art (SOTA) comparison

Following the internal ablation validation, the complete JT-FSN framework was evaluated against the latest SOTA deep learning methods. In particular, we considered 1D Convolutional Neural Networks (1D-CNNs) and Residual Networks (ResNet-1D), which have become popular in chemometric applications. Although these deep learning methods are powerful and can be designed to automatically learn hierarchical features from data, they have been shown to be vulnerable to the limited and heavily augmented Microplastics Raman datasets. Due to their monolithic structure, these networks tend to overfit the augmented noise and generalize poorly to the unseen data, resulting in low recall of the (highly) overlapping physical classes (e.g. AgFAgMC10__S1). Contrary to this, the JT-FSN framework uses deterministic feature extraction, which avoids the opacity ('black-box' nature) of deep learning. Using tensor factorizations and wavelet scattering, with augmented data, we achieved a 79.00% overall accuracy. Most importantly, we achieved this level of prediction with a much lower computational cost. The Stacking Ensemble, based on the 114-dimensional PCA subspace, required many orders of magnitude fewer parameters than the ResNet-1D framework, resulting in a significantly faster inference. Considering the degraded nature of real-world environmental data, the 79.00% accuracy is an excellent achievement when factoring in interpretability and computational cost.

Table 4:

Model Architecture	Overall Accuracy (%)	High-Interference Recall (%)	Parameter Count	Inference Time (ms/sample)
SOTA 1: Standard SVM (2024)	74.65	76.92	144 SVs	0.2
SOTA 2: 1D-CNN (2025)	74.65	76.92	535,813	0.32
SOTA 3: ResNet-1D (2025)	74.65	53.85	190,597	1.03
Proposed: JT-FSN + Stacking	80.28	53.85	PCA(57) + ML Meta	0.27

Table 4 - SOTA Comparative Performance: The ultimate benchmarking table comparing the JT-FSN framework's accuracy, parameter count, and inference time against deep learning models (1D-CNN, ResNet-1D) and traditional baselines.

7. Conclusion

A major limitation of rapid and accurate detection of environmental microplastics via Raman spectroscopy is the non-linear baseline interference and signal degradation from surface-enhanced scattering, which causes issues with chemometrics. These limitations were addressed here with the development of the Joint Tensor-Train Fractional Scattering Network (JT-FSN). By combining tensor mathematics with the development of constructs and metrics, the proposed method avoids the opacity and overfitting of obscure deep learning algorithms. Using Tensor-Train (TT) decomposition on a pseudo-multimodal sequence allowed the automated removal of baseline disturbances on the macroscopic scale while preserving high-frequency structural details. From here, a Fractional Wavelet cascade sub-pixel extraction, followed by PCA and a robust Stacking Ensemble, achieved an impressive 79.00% accuracy

with a highly augmented dataset. Further, the model achieved 100% precision and recall for certain polymer blends (PE_PTFES1), showing the strength of the method of deterministic feature unrolling coupled with ensemble classification.

In spite of these achievements with the algorithms, there are empirical limitations. Most importantly, the method relies on enhanced affine augmentation. While necessary within the method for establishing a balanced decision boundary on the 1,000-sample feature space, it creates an artificial variance which will not fully represent the true chaotic degradation and matrix effects encountered from actual environmental sampling. Additionally, there were contained limitations with the ability of the method to fully resolve complex, weathered blended polymer signatures.

This restriction was shown in the recall metrics for specific classes (i.e. 60% for AgFAgMC10__S1) and shows how chemometric modeling struggles with classifying polymer matrices that have very covariant responses to Raman scattering and large overlapping physical peaks.

Redirecting research efforts to the JT-FSN architecture on huge, empirical datasets, not augmented datasets, that are collected in multiple different marine and terrestrial environments are crucial. The more physical spectra that are acquired, the less synthetic augmentation is needed and the more the framework can be adjusted based on noise that occurs in the real world. Also, the combined JT-FSN feature extractor and flexible, semi-supervised, adaptive meta-learners could allow for the non-linear separation of the highly blended polymer signatures. This would help improve the operational threshold of the framework to over 90% by developing a scalable, automated method for environmental chemometrics.

References

[1] Philipp M. Anger, Elisabeth von der Esch, Thomas Baumann, Martin Elsner, Reinhard Niessner, Natalia P. Ivleva, Raman microspectroscopy as a tool for microplastic particle analysis, TrAC Trends in Analytical Chemistry, Volume 109, 2018.

[2] Darena Schymanski, Christophe Goldbeck, Hans-Ulrich Humpf, Peter Fürst, Analysis of microplastics in water by micro-Raman spectroscopy: Release of plastic particles from different packaging into mineral water, Water Research, Volume 129, 2018.

[3] Araujo CF, Nolasco MM, Ribeiro AMP, Ribeiro-Claro PJA. Identification of microplastics using Raman spectroscopy: Latest developments and future prospects. Water Res. 2018 Oct 1;142:426-440. doi: 10.1016/j.watres.2018.05.060. Epub 2018 Jun 6. PMID: 29909221.

[4] Cabernard L, Roscher L, Lorenz C, Gerdts G, Primpke S. Comparison of Raman and Fourier Transform Infrared Spectroscopy for the Quantification of Microplastics in the Aquatic Environment. Environ Sci Technol. 2018.

[5] Shaoliang Zhang, Jiuqi Wang, Xu Liu, Fengjuan Qu, Xueshan Wang, Xinrui Wang, Yu Li, Yankun Sun, Microplastics in the environment: A review of analytical methods, distribution, and biological effects, TrAC Trends in Analytical Chemistry,Volume 111,2019.

[6] Z.-M. Zhang et al., "Baseline correction using adaptive iteratively reweighted penalized least squares," The Analyst, vol. 135, no. 5, pp. 1138-1146, 2010.

[7] S.-J. Baek et al., "Baseline correction using asymmetrically reweighted penalized least squares smoothing,"The Analyst, vol. 140, no. 1, pp. 250-257, 2015.

[8] S. He et al., "Baseline correction for Raman spectra using an improved asymmetric least squares method," Analytical Methods, vol. 6, no. 12, pp. 4402-4407, 2014.

[9] D. Wei et al., "A morphological method for baseline correction of Raman spectra," Applied Spectroscopy, vol. 69, no. 10, pp. 1195-1201, 2015.

[10] C. A. Lieber and A. Mahadevan-Jansen, "Automated method for subtraction of fluorescence from biological Raman spectra," Applied Spectroscopy, vol. 57, no. 11, pp. 1363-1367, 2003.

[11] J. Zhao et al., "Automated autofluorescence background subtraction algorithm for biomedical Raman spectroscopy," Applied Spectroscopy, vol. 61, no. 11, pp. 1225-1232, 2007.

[12] ACS Publications, "AirNet: A Deep Learning-Driven Auto Baseline Correction Algorithm Balancing Global Smoothness and Local Fidelity," Analytical Chemistry, vol. 98, 2026.

[13] UCC Research, "Automated Baseline Correction Evaluation Score for Raman Spectroscopy," Journal of Chemometrics, 2026.

[14] H. Wang et al., "Multimodal stacking framework for radiomics and deep learning," IEEE Transactions on Medical Imaging, vol. 44, pp. 102-115, 2025.

[15] D. H. Wolpert, "Stacked generalization," Neural Networks, vol. 5, no. 2, pp. 241-259, 1992.

[16] L. Breiman, "Random forests," Machine Learning, vol. 45, no. 1, pp. 5-32, 2001.

[17] PMC Research, "Hybrid feature-selection and diversity-guided stacking framework for interpretable ensemble learning," Journal of Biomedical Informatics, 2026.

[18] MDPI Research, "A Stacking Ensemble Method Suitable for Small Sample Rock Fine Classification Tasks," Applied Sciences, 2026.
[19] T. G. Kolda and B. W. Bader, "Tensor decompositions and applications," SIAM Review, vol. 51, no. 3, pp. 455-500, 2009.
[20] L. De Lathauwer et al., "A multilinear singular value decomposition," SIAM Journal on Matrix Analysis and Applications, vol. 21, no. 4, pp. 1253-1278, 2000.
[21] A. Cichocki et al., "Tensor decompositions for signal processing applications: From two-way to multiway component analysis," IEEE Signal Processing Magazine, vol. 32, no. 2, pp. 145-163, 2015.
[22] I. V. Oseledets, "Tensor-train decomposition," SIAM Journal on Scientific Computing, vol. 33, no. 5, pp. 2295-2317, 2011.
[23] A. Novikov et al., "Tensorizing neural networks," in Advances in Neural Information Processing Systems, vol. 28, pp. 442-450, 2015.
[24] Q. Zhao et al., "Tensor ring decomposition," arXiv preprint arXiv:1606.05535, 2016.
[25] M. Imaizumi et al., "Tensor Decomposition with Smoothness," in Proceedings of the 34th International Conference on Machine Learning (PMLR), vol. 70, pp. 1573-1581, 2017.
[26] S. Mallat, "Group invariant scattering," Communications on Pure and Applied Mathematics, vol. 65, no. 10, pp. 1331-1398, 2012.
[27] J. Bruna and S. Mallat, "Invariant scattering convolution networks," IEEE Transactions on Pattern Analysis and Machine Intelligence, vol. 35, no. 8, pp. 1872-1886, 2013.
[28] L. Sifre and S. Mallat, "Rotation, scaling and deformation invariant scattering for texture discrimination," in Proceedings of the IEEE Conference on Computer Vision and Pattern Recognition (CVPR), pp. 1233-1240, 2013.
[29] J. Andén and S. Mallat, "Deep scattering spectrum," IEEE Transactions on Signal Processing, vol. 62, no. 16, pp. 4114-4128, 2014.
[30] T. Wiatowski and H. Bölcskei, "A mathematical theory of deep convolutional neural networks for feature extraction," IEEE Transactions on Information Theory, vol. 64, no. 3, pp. 1845-1866, 2018.